J Ind Microbiol Biotechnol (2014) 41:1217–1225
DOI 10.1007/s10295-014-1463-y

BIOTECHNOLOGY METHODS

SIMB
Society for Industrial Microbiology and Biotechnology

Improving the thermostability of a mesophilic family 10 xylanase, AuXyn10A, from *Aspergillus usamii* by in silico design

Junqing Wang · Zhongbiao Tan · Minchen Wu · Jianfang Li · Jing Wu

Received: 20 February 2014 / Accepted: 9 May 2014 / Published online: 31 May 2014

Abstract To improve the thermostability of a mesophilic GH family 10 xylanase, AuXyn10A, from *Aspergillus usamii* E001, its modification was performed by in silico design. Based on the comparison of B-factor values, a mutant xylanase ATXyn10 was predicted by substituting a segment YP from Tyr^{25} to Pro^{34} of AuXyn10A with the corresponding one from Asn^{24} to Ala^{32} of TaXyn10, a thermophilic GH family 10 xylanase from *Thermoascus aurantiacus*. Analysis of a TaXyn10 crystal structure indicated that there is a close interaction between segments YP and FP. For that reason, another mutant xylanase $ATXyn10^{M}$ was designed by mutating Ser^{286} and His^{288} of ATXyn10 into the corresponding Gly^{285} and Phe^{287} in the FP of TaXyn10. Then, two ATXyn10- and $ATXyn10^{M}$-encoding genes, *ATxyn10* and $ATxyn10^{M}$, were expressed in *Pichia pastoris* GS115. The temperature optimum of recombinant (re) $ATXyn10^{M}$ was 60 °C, 10 °C higher than that of reAuXyn10A. Its thermal inactivation half-life ($t_{1/2}$) at 55 °C was 10.4-fold longer than that of reAuXyn10A. As compared with reAuXyn10A, $reATXyn10^{M}$ displayed a slight decrease in K_m value and a significant increase in V_{max} value from 6,267 to 8,870 U/mg.

Keywords Xylanase · Thermostability · Segment substitution · Site-directed mutagenesis · *Aspergillus usamii*

J. Wang and Z. Tan, the two first authors, contributed equally to this work.

J. Wang · M. Wu
Key Laboratory of Carbohydrate Chemistry and Biotechnology, Ministry of Education, Jiangnan University, 1800 Lihu Road, Wuxi 214122, Jiangsu, People's Republic of China

J. Wang · Z. Tan
Key Laboratory of Industrial Biotechnology, Ministry of Education, School of Biotechnology, Jiangnan University, 1800 Lihu Road, Wuxi 214122, Jiangsu, People's Republic of China

M. Wu · J. Wu
Wuxi Medical School, Jiangnan University, Wuxi 214122, Jiangsu, China

M. Wu (✉)
School of Medicine and Pharmaceutics, Jiangnan University, 1800 Lihu Road, Wuxi 214122, Jiangsu, People's Republic of China
e-mail: biowmc@126.com

J. Li
State Key Laboratory of Food Science and Technology, School of Food Science and Technology, Jiangnan University, Wuxi 214122, Jiangsu, China

Introduction

Xylan is a heteroglycan, which contains a backbone made up of β-1,4-D-linked xylose residues with substitutions of L-arabinofuranosyl, 4-*O*-methyl-D-glucuronosyl and acetyl groups at C-2 and/or C-3 positions [1]. The complete degradation of xylan requires a variety of synergistically acting xylanolytic enzymes. Among them, xylanase (endo-β-1,4-D-xylanase, EC 3.2.1.8) is an important enzyme in that it catalyzes the hydrolysis of internal β-1,4-D-xylosidic linkages of xylan via a double displacement mechanism, in which two conserved glutamic acids act as a general acid catalyst and a nucleophile [18]. Based on the hydrophobic cluster analysis and homology alignment of primary structures, the majority of xylanases have been grouped into glycoside hydrolase (GH) families 10 and 11 [16]. In striking contrast to GH family 11 counterparts, the family 10 xylanases exhibit higher molecular masses (>30 kDa) and lower substrate specificities, and possess catalytic activities towards some cellulosic substrates, such as aryl

cellobiosides [3]. The overall three-dimensional (3-D) structure of GH family 10 xylanases consists principally of a $(\beta/\alpha)_8$ barrel fold, resembling the shape of a 'salad bowl' [5].

Currently, thermophilic xylanases have been applied in industrial processes where the cooling step is uneconomical, and where high temperature is required to improve the availability and solubility of substrates and to reduce the viscosity of solution and the risk of microbial contamination. However, the majority of wild-type xylanases have thermostability [4]. Although a handful of thermophilic xylanases were produced from thermophiles, their expression levels and specific activities were much lower [23, 28], making them unable to be applied efficiently. For those reasons, it was highly desirable to improve the thermostability of mesophilic xylanases with higher specific activity by genetic engineering. Some domains or local structures affecting the thermostability of xylanases have been elucidated through analyzing and comparing the primary and/or 3-D structures of mesophilic xylanases with those of the corresponding thermophilic ones [6, 10].

The full-length cDNA and complete DNA sequences of a GH family 10 xylanase gene, *Auxyn10A*, from *Aspergillus usamii* E001 were analyzed [27]. Then, *Auxyn10A* was expressed in *Pichia pastoris* GS115, and the properties of expressed reAuXyn10A were characterized, displaying the high specific activity, broad pH stability and strong tolerance to metal ions and EDTA, except poor thermostability [26]. The primary structure homology alignment showed that AuXyn10A shared 73.3 % identity with TaXyn10, a thermophilic family 10 xylanase [24]. In this work, two mutant xylanases, ATXyn10 and ATXyn10^{M}, were designed by replacing a segment of AuXyn10A with the corresponding one of TaXyn10 and by mutating two amino acids of ATXyn10, respectively. Then, one wild-type xylanase gene *Auxyn10A* and two mutant xylanase genes *ATxyn10* and *ATxyn10*^{M} were expressed in *P. pastoris*, respectively. The enzymatic properties, especially the temperature optima and thermostabilities, of reAuXyn10A, reATXyn10 and reATXyn10^{M} were characterized and compared. Although this approach was successfully used to improve the thermostability of GH family 11 xylanases in our previous reports [9, 29], considering the huge difference between GH family 10 xylanases and 11 xylanases, this work is still meaningful and can be used for guiding the thermostability improvement of those xylanses with $(\beta/\alpha)_8$ barrel fold structures.

Materials and methods

Strains, vectors and culture media

Both the recombinant T-vector (pUCm-T-*Auxyn10A*) and *P. pastoris* transformant (GSX10A4-14) containing *Auxyn10A* were constructed and preserved in our lab [26]. *Escherichia coli* JM109 and vector pUCm-T (Sangon, Shanghai, China) were used for gene cloning, while *E. coli* DH5α and vector pPIC9K^{M} for construction of the recombinant expression vector. The pPIC9K^{M} was built in our lab from pPIC9K (Invitrogen, San Diego, CA), which could make a recombinant protein in *P. pastoris* retaining the N-terminus from the native protein [26]. *E. coli* JM109 and DH5α were cultured in the LB medium, while *P. pastoris* GS115 and its transformant cultured and induced in the YPD, MD, geneticin G418-containing YPD, BMGY and BMMY media. All the culture media were prepared as described in the manual of Multi-Copy Pichia Expression Kit (Invitrogen).

Analysis of the xylanase primary and 3-D structures

The homology sequence search at the NCBI website (http://www.ncbi.nlm.nih.gov/) in Protein Data Bank (PDB) was performed using the BLAST server, while the homology alignment among family 10 xylanase primary structures was done using the ClustalW2 program (http://www.ebi.ac.uk/Tools/msa/clustalw2/) and DNAMAN 6.0 software. Three known crystal structures of family 10 xylanases from *Thermoascus aurantiacus* (PDB: 2BNJ), *Penicillium simplicissimum* (PDB: 1BG4) and *Emericella nidulans* (PDB: 1TA3), which share high primary structure identities with AuXyn10A, were selected as the templates. The 3-D structure of xylanase was predicted by multiple template-based homology modeling using the SALIGN program (http://salilab.org/DBAli/?page=tools_&action=f_salign) and the MODELLER 9.9 program (http://salilab.org/modeller/) [8]. The polar surface area (PSA) of xylanase was calculated using the GetArea program (http://curie.utmb.edu/getarea.html), while the intramolecular interaction was identified using the PIC server (http://pic.mbu.iisc.ernet.in/).

Computational prediction for the xylanase thermostability

After the protein 3-D structure was subjected to molecular dynamics (MD) simulation, the B-factor values, namely atomic displacement parameters, of amino acids were generated and calculated using the GROMACS 4.5 package (http://www.gromacs.org/) and B-FITTER program [21], respectively. In this work, the 3-D structures of AuXyn10A and TaXyn10 were subjected to 15 ns MD simulations at 300 K, respectively, for calculating the B-factor values. Based on the comparison of B-factor values between them, ATXyn10 was designed by substituting a segment Y^{25}TLTKDSKTP^{34} of AuXyn10A with the corresponding N^{24}RLTTGKNA^{32} of TaXyn10. Meanwhile, ATXyn10^{M} was predicted by mutating Ser^{286} and His^{288} of ATXyn10 into Gly and Phe, respectively, through analyzing and

comparing the primary and 3-D structures of ATXyn10 and TaXyn10.

The root mean square deviation (RMSD) value, an index for evaluating the thermal fluctuation, was defined as the C_α-atomic displacement range of a protein from its original conformation to the changed one at a high temperature and a certain time, which has a negative correlation with the thermostability [2]. To evaluate the thermostability of AuXyn10A, ATXyn10 and ATXyn10^M, their 3-D structures were subjected to MD simulations, respectively, at 500 K for 8 ns. The RMSD values were calculated using a g_rms software of the GROMACS 4.5 package, and statistically analyzed using an Origin 9 software (http://www.originlab.com/).

Assessment of the variability of xylanase secondary structures

The thermostability of a protein, closely correlated with its conformation diversification at a high temperature, could be evaluated by using the 'defined secondary structure of proteins' (DSSP) method [12]. The 3-D structures of AuXyn10A and ATXyn10^M here were subjected to MD simulations, respectively, at 500 K for 5 ns. Then, the variability of secondary structures, such as helix (α-helix, π-helix and 3′-helix) and strand (β-sheet and β-bridge), was assessed by DSSP program (http://swift.cmbi.ru.nl/gv/dssp/).

Construction of the mutant xylanase genes

ATxyn10 was amplified from pUCm-*Auxyn10A* by megaprimer PCR [17]. The first-round PCR for the DNA fragment *AT* was performed with AuX-F (5′-CTCGAGAAAAGACAGGCTTCAGTGAGTATTGA-3′ having an oligonucleotide 5′-CTCGAGAAAAGA-3′ with an *Xho*I site, underlined) and AT-R (5′-TGATAATGGCCGCATTCTTGCCGGTCGTCAGCCGGTTCTGATCACCAAT-3′). Conditions for first-round PCR were: a denaturation at 94 °C for 3 min; 30 cycles of at 94 °C for 30 s, 55 °C for 30 s, 72 °C for 15 s; an elongation at 72 °C for 10 min. Next, the second-round PCR for *ATxyn10* was carried out with *AT* and AuX-R (5′-GCGGCCGCCTAGAGAGCATTTGCGATAG-3′ with a *Not*I site, underlined) under the same conditions, except at 72 °C for 60 s in 30 cycles.

ATxyn10^M was constructed by mutating Ser^{286}- and His^{288}-encoding codons of *ATxyn10* into Gly- and Phe-encoding ones, respectively. Using pUCm-*ATxyn10* as the template, the fragment *AT*^{M} was first amplified with AT^M-F (5′-GCTGTTCGACGGCAACTTCAACCCGAAGC-3′ with mutant codons, boxed) and AuX-R, and then *ATxyn10*^{M} amplified with AuX-F and *AT*^{M}. The target PCR products were gel-purified, inserted into pUCm-T and transformed into *E. coli* JM109, respectively. The recombinant T-vectors, pUCm-T-*ATxyn10* and -*ATxyn10*^{M}, were confirmed by DNA sequencing.

Expression of the xylanase genes

Both *ATxyn10* and *ATxyn10*^{M} were excised from pUCm-T-*ATxyn10* and -*ATxyn10*^{M} by digestion with *Xho*I and *Not*I, and inserted into vector pPIC9K^M digested with the same enzymes, followed by transforming them into *E. coli* DH5α, respectively. Then, the resulting recombinant expression vectors, pPIC9K^M-*ATxyn10* and -*ATxyn10*^{M}, were linearized with *Sal*I and transformed into *P. pastoris* GS115 on a Gene Pulser apparatus (Bio-Rad, Hercules, CA). *P. pastoris* GS115 transformed with pPIC9K^M was used as the negative control (*P. pastoris* GSC). *P. pastoris* transformants were picked out based on their ability to grow on an MD plate, and inoculated successively on G418-containing YPD plates at increasing concentrations for screening multiple copies of integrated *ATxyn10* and *ATxyn10*^{M}, respectively. Expression of the gene in *P. pastoris* GS115 was performed according to the method as reported previously [26].

Enzyme activity and protein assays

Xylanase activity was assayed by incubating 100 μl of suitably diluted enzyme with 2.4 ml of 0.5 % (w/v) birchwood xylan (Sigma, St. Louis, MO) in 50 mM Na_2HPO_4–citric acid buffer (pH 5.5) at 50 °C for 15 min [26]. One unit (U) of xylanase activity was defined as the amount of enzyme liberating 1 μmol of reducing sugar equivalent per min under the assay conditions. The sodium dodecyl sulfate–polyacrylamide gel electrophoresis (SDS-PAGE) was performed on a 12.5 % gel. The protein concentration was measured with the BCA-200 Protein Assay Kit (Pierce, Rockford, IL).

Purification of the recombinant xylanases

A total of 50 ml of cultured supernatant was brought to 75 % saturation by adding solid $(NH_4)_2SO_4$. The precipitate was harvested, dissolved in 5 ml of 20 mM Na_2HPO_4–NaH_2PO_4 buffer (pH 6.0), and dialyzed against the same buffer overnight. The dialysate was concentrated to 1 ml by ultrafiltration with a 10-kDa cut-off membrane (Millipore, Billerica, MA), and loaded onto a carboxymethyl cellulose CM-52 cation exchange column (Whatman, Maidstone, UK; 1.6 × 20 cm), followed by elution with a linear gradient of 0–0.5 M NaCl in the same buffer at a flow rate of 0.4 ml/min. Aliquots of 2 ml eluent only containing the target xylanase were pooled, dialyzed against deionized water and concentrated. All purification procedures were performed at 4 °C unless stated otherwise.

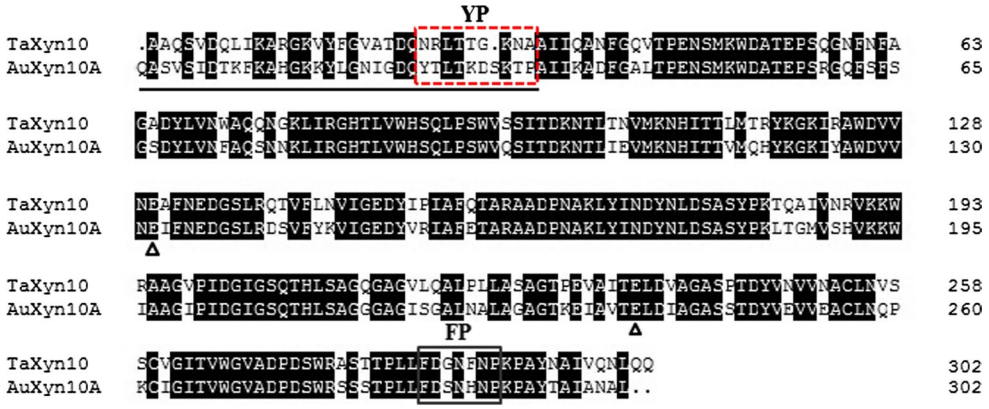

Fig. 1 The homology alignment of amino acid sequences between xylanases TaXyn10 and AuXyn10A. *TaXyn10* a thermophilic GH family 10 xylanase from *T. aurantiacus*, *AuXyn10A* a mesophilic counterpart from *A. usamii*. The identical amino acid residues between them are marked in *black background*. Two conserved glutamic acids are indicated in *triangles*, which act as a general acid catalyst and a nucleophile, respectively. N-terminal 44 amino acid residues (numbered by AuXyn10A) of both TaXyn10 and AuXyn10A are *underlined*

Temperature optimum and thermostability

The temperature optimum of the recombinant xylanase was measured under the standard xylanase activity assay conditions, except temperatures ranged from 40 to 70 °C. To evaluate the thermostability, xylanase was incubated in the absence of substrate at 50, 55 and 60 °C for 80 min. The thermal inactivation half-life was defined as a time when the residual xylanase activity, measured under the standard assay conditions, retained 50 % of its original activity.

Enzymatic kinetic parameters

The hydrolytic reaction rate (μmol/min/mg) of xylanase was measured under the standard assay conditions, except birchwood xylan concentrations ranged from 1.0 to 10 mg/ml. The reaction rate versus substrate concentration was plotted to confirm whether the hydrolytic mode of reATXyn10 or reATXyn10^{M} conforms to the Michaelis–Menten equation. The kinetic parameters, K_m and V_{max}, were graphically determined from the Lineweaver–Burk plotting.

Results and discussion

Homology alignment between the mesophilic and thermophilic xylanases

The thermophilic GH family 10 xylanase TaXyn10 from *Thermoascus aurantiacus*, which shares the highest identity with the mesophilic counterpart AuXyn10A, was searched at the NCBI website using the BLAST server. Then, the homology alignment, conducted by using the ClustalW2 program, displayed that the primary structure of TaXyn10 shared 73.3 % identity with that of AuXyn10A, but the identity of N-terminal 44 amino acid residues between them (numbered by AuXyn10A) was as low as 45.4 % (Fig. 1). That, to some extent, implied the significance of the N-terminal region of TaXyn10 to its high thermostability.

Computational prediction for the xylanase thermostability

It was demonstrated that the 3-D structure of a mesophilic protein is more flexible than that of a thermophilic one [11]. To quantify the protein flexibility, the notion of B-factor values was introduced to reflect smearing of atomic electron densities as a result of thermal motion and positional disorder [22]. The B-factor values of AuXyn10A and TaXyn10 here were calculated, respectively (Fig. 2a). After comparing the B-factor values between them, YP (a region with obvious different B-factor values between AuXyn10A and TaXyn10 at N-terminal) from Tyr^{25} to Pro^{34} of AuXyn10A was selected, corresponding to more pronounced degrees of thermal motion, that is, flexibility. Then, ATXyn10 was designed by replacing the YP of AuXyn10A with the corresponding one from Asn^{24} to Ala^{32} of TaXyn10. In addition, analysis of the crystal structure of TaXyn10 (PDB: 2BNJ) using the PIC server indicated that there is a close interaction between YP and FP (a region in direct contact with YP) of TaXyn10 (Fig. 2b); moreover, the α-helixes of TaXyn10 were formed as a cycle around internal β-strands, the FP and YP were in this outside cycle and on the opposite side of the joint (Fig. 2c). These results suggested that the FP and YP may be closely associated with its thermostability. For that reason, ATXyn10^{M} was predicted by mutating Ser^{286} and His^{288} of ATXyn10 into

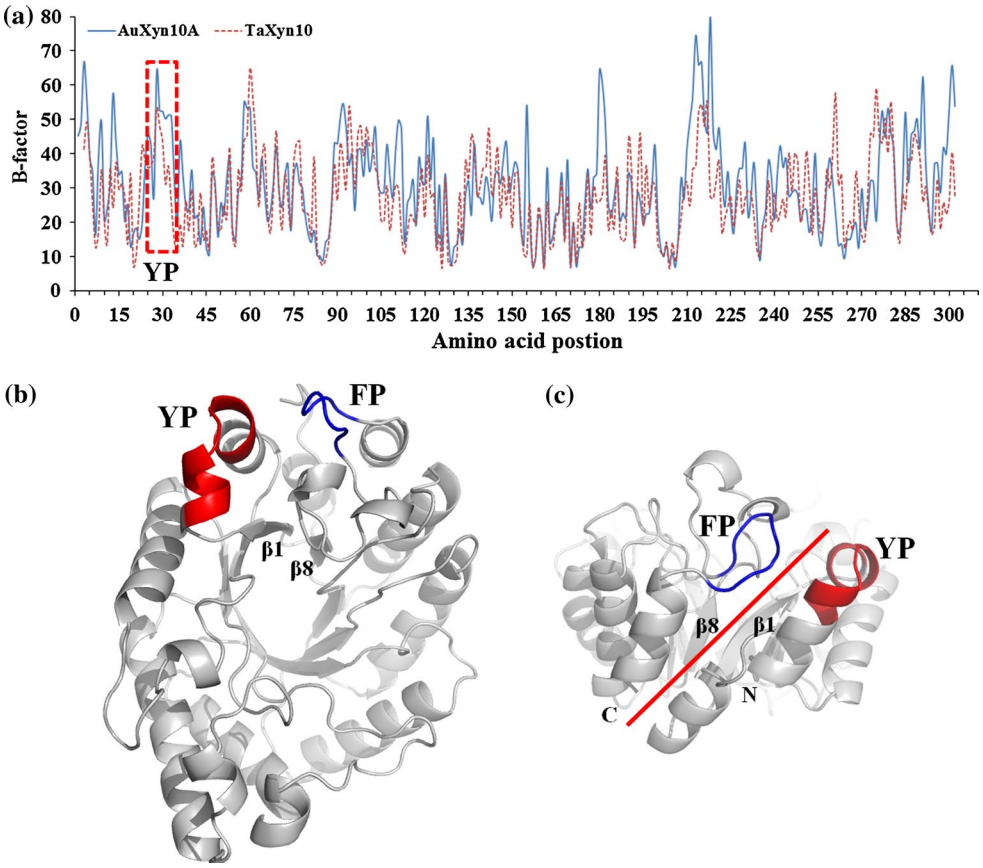

Fig. 2 Determination of the sites for both segment substitution and site-directed mutagenesis based on the in silico design. **a** The B-factors of amino acids of AuXyn10A and TaXyn10 are marked in *solid* and *dashed lines*, respectively. The region YP for segment substitution is *boxed* with *dashed line*. **b** *Top view* of the crystal structure of TaXyn10 (PDB: 2BNJ). Analysis of TaXyn10 crystal structure using the PIC server indicated that there is a close interaction between regions YP and FP. **c** *Stereo view* of TaXyn10 along the barrel axis. The *red line* represents the joint between the β1-strand and β8-strand of TaXyn10

the corresponding Gly^{285} and Phe^{287} in the FP of TXyn10, respectively.

The 3-D structures of AuXyn10A, ATXyn10 and ATXyn10^{M} were subjected to MD simulations at 500 K, followed by calculating their RMSD values, respectively. Although 500 K is experimentally unrealistic, the MD simulation at this temperature gives an insight into protein unfolding [19]. As shown in Fig. 3a, the RMSD values of ATXyn10^{M} after equilibration were smaller than those of AuXyn10A. Besides, the RMSD values of ATXyn10^{M} were mainly focused on 0.58 nm while those of AuXyn10A on 0.79 nm (Fig. 3b), indicating that ATXyn10^{M} was more rigid than AuXyn10A. Based on the analytical result that the rigidity of a protein was positively related to its thermostability [20], ATXyn10^{M} was evaluated to be more thermostable than AuXyn10A.

Assessment of the secondary structure variability

The diversifications of helix and strand conformations of AuXyn10A, ATXyn10 and ATXyn10^{M} were assessed, respectively. At the beginning of MD simulation, AuXyn10A statistically consisted of ~61 % helix and ~26 % strand, while ATXyn10^{M} was ~58 % helix and ~23 % strand. During the simulation process, the variation trajectory of the helix content of AuXyn10A was almost equal to that of ATXyn10^{M} (Fig. 4a). The strand content of AuXyn10A gradually decreased to ~15 %, while that of ATXyn10^{M} almost kept the same level (Fig. 4b), suggesting that the unfolding of ATXyn10^{M} is less obvious than that of AuXyn10A. However, compared with ATXyn10^{M}, the general unfolding trend of ATXyn10 was almost equal to that of AuXyn10A in the whole MD simulation, suggesting that the substitution of YP might have affected the thermostability of AuXyn10A less. Synthesizing the above results, the substitution of YP together with mutations of Ser^{286} and His^{288} made the conformation of ATXyn10^{M} more stable at a high temperature, which may contribute to its elevated thermostability. The DSSP method has been extensively used to assess or predicted the thermostability of proteins or enzymes [2].

Construction of the mutant xylanase genes

An about 150-bp band of *AT* was amplified from pUCm-T-*Auxyn10A* by first-round PCR with AuX-F and AT-R. Next, a 900 bp of *ATxyn10* was amplified by second-round PCR with *AT* and AuX-R. The DNA sequencing result demonstrated that the DNA fragment coding for YP of AuXyn10A was substituted by the corresponding one of TaXyn10.

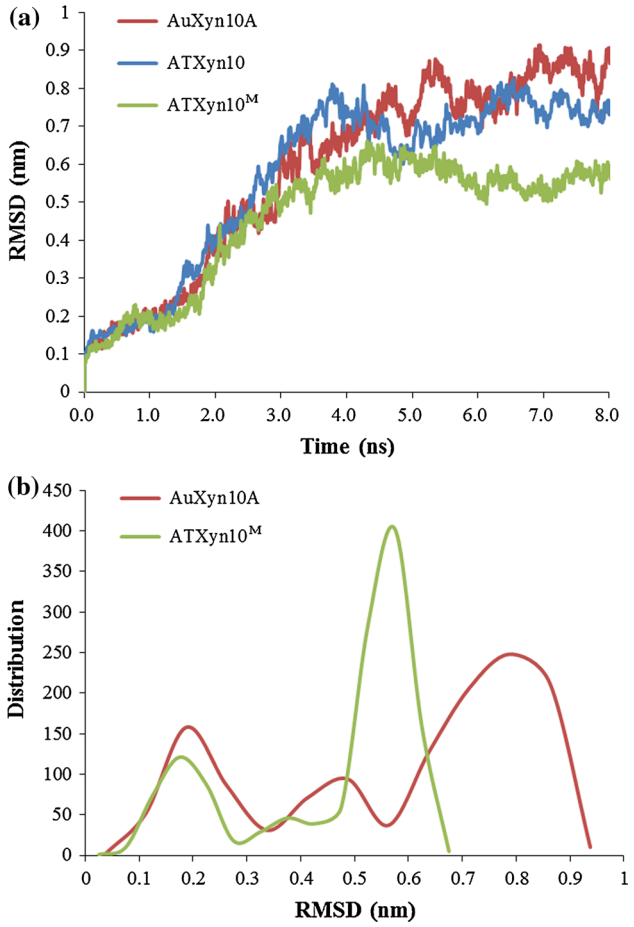

Fig. 3 Calculation and distribution of the RMSD values. **a** Curves of RMSD values of AuXyn10A (*red*), ATXyn10 (*blue*) and ATXyn10^{M} (*green*) after MD simulations at 500 K for 8 ns. **b** Distributions of RMSD values of both AuXyn10A (*red*) and ATXyn10^{M} (*green*)

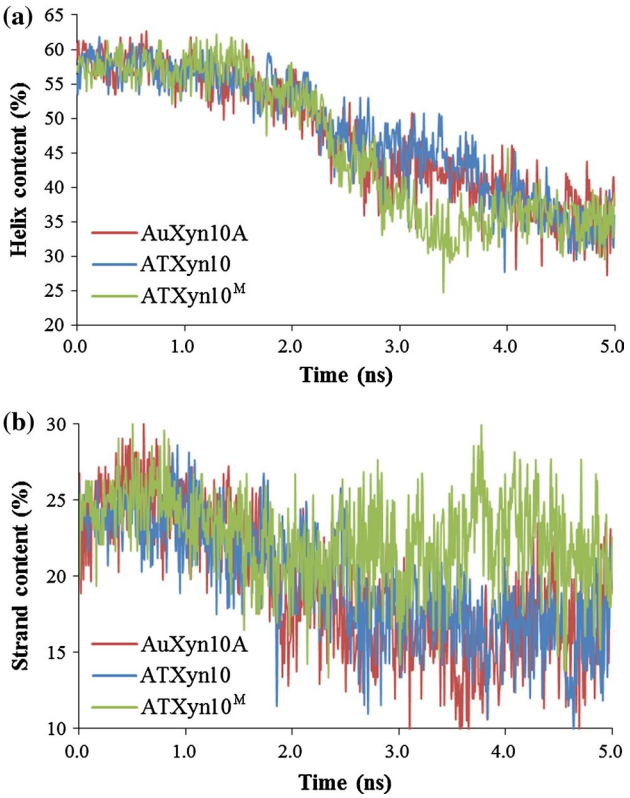

Fig. 4 Assessment of the secondary structure variability. **a** The helix contents of AuXyn10A (*red*), ATXyn10 (*blue*) and ATXyn10^{M} (*green*) were assessed, respectively, using the DSSP program after MD simulations at 500 K for 5 ns. **b** The strand contents of AuXyn10A (*red*), ATXyn10 (*blue*) and ATXyn10^{M} (*green*)

In addition, using pUCm-T-*ATxyn10* as the template, an approximate 100-bp *AT*^{M} was amplified with AT^{M}-F and AuX-R, and then a 900 bp of *ATxyn10*^{M} amplified with AuX-F and *AT*^{M}. The DNA sequencing result verified that the cloned *ATxyn10*^{M} did mutate Ser^{286}- and His^{288}-encoding codons (AGC and CAC) of *ATxyn10* into Gly- and Phe-encoding ones (GGC and TTC), respectively, as designed theoretically.

Expression and purification of the recombinant xylanases

The *P. pastoris* transformant that can resist higher concentrations of G418 (Geneticin) may contain multiple copies of integration of the heterologous gene into *P. pastoris* genome, potentially leading to a higher expression level of a heterologous protein as elucidated in the manual of Multi-Copy Pichia Expression Kit (Invitrogen). But, the expression level was not directly proportional to the concentration of G418 [14]. For those reasons, *P. pastoris* transformants

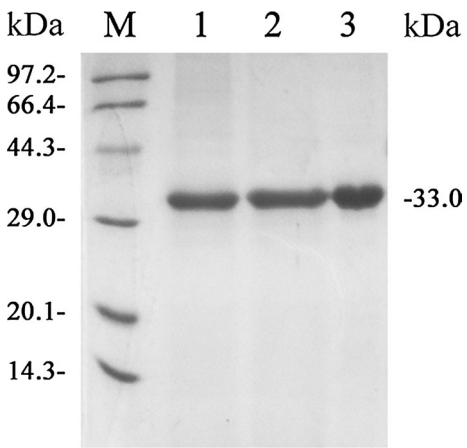

Fig. 5 SDS-PAGE analysis of the purified xylanases. *Lanes M* protein marker, *1, 2, 3* purified reAuXyn10A, ATXyn10 and ATXyn10^{M} with apparent molecular mass of ~33.0 kDa

separately resistant to 1.0, 2.0 and 4.0 mg/ml of G418, were picked out for flask tests. Two of tested transformants, labeled as *P. pastoris* GSATX4-3 and GSATX^{M}4-17,

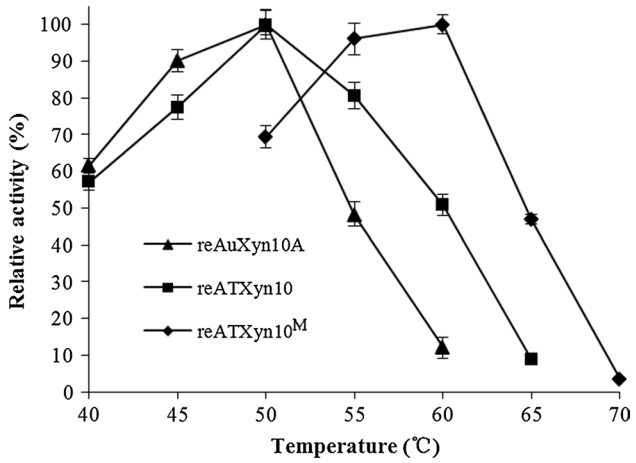

Fig. 6 Effect of temperature on the recombinant xylanase catalytic activity. The temperature optima of reAuXyn10A, reATXyn10 and reATXyn10^{M} were measured, respectively, under the standard xylanase activity assay conditions, except temperatures ranging from 40 to 70 °C

having the highest reATXyn10 and reATXyn10^{M} activities of 100.8 and 521.9 U/ml, respectively, were screened. The recombinant xylanase was then purified to homogeneity by a simple combination of ammonium sulfate precipitation, ultrafiltration and cation exchange chromatography, showing a single protein band on SDS-PAGE (Fig. 5).

Temperature properties of three recombinant xylanases

The temperature optima of both reAuXyn10A and reATX10A were 50 °C (measured at pH 5.5 for 10 min), while that of reATX10A^{M} was 60 °C (Fig. 6). The reATX10A^{M} was highly stable (more than 90 % of its original activity) at 50 °C for 80 min (Fig. 7a), whereas the reAuXyn10A was stable only at 45 °C [26]. Although the temperature optima of reATX10A^{M} was not up to the level of TaXyn10 (80 °C) [15], it displayed a significant increase of thermostability as compared with reAuXyn10A. The thermal inactivation half-lives ($t_{1/2}$) of reAuXyn10A, reATX10A and reATX10A^{M} at 55 °C were 6.9, 8.0 and 72 min, respectively (Fig. 7b). These results revealed that the thermostability of AuXyn10A was increased more significantly using the method combining segment substitution with site-directed mutagenesis than using the segment substitution alone.

Enzymatic substrate specificity and kinetic parameters

The reAuXyn10A, reATX10A or reATX10A^{M} had the highest specific activity towards birchwood xylan (defined as 100 %), followed by corncob xylan (84.1 %) and beechwood xylan (61.3 %). No xylanase activity was detected

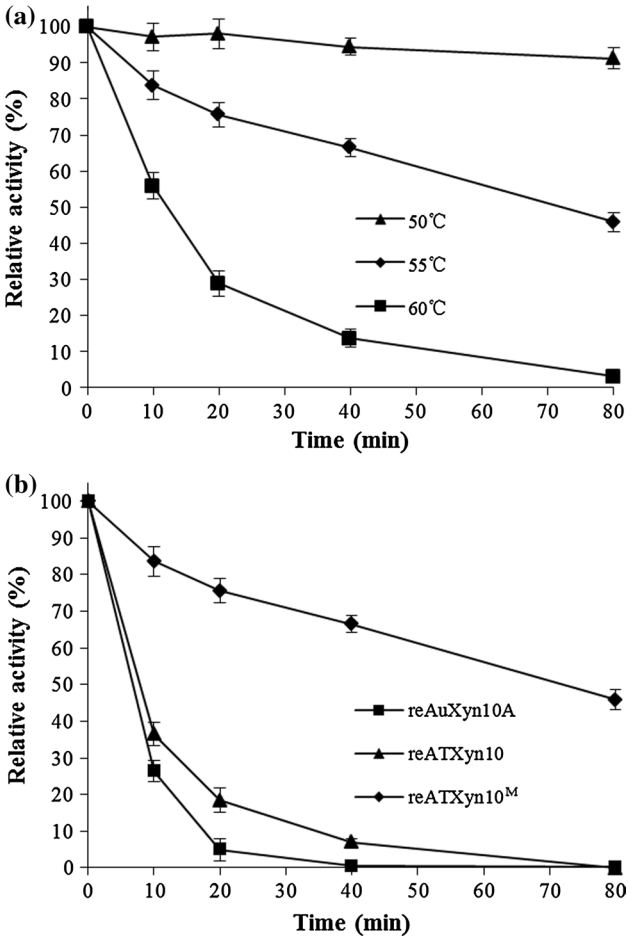

Fig. 7 Thermostability of the recombinant xylanases. **a** To evaluate the thermostability, reAuXyn10A was incubated at 50, 55 and 60 °C, respectively, in 80 min. **b** The thermal inactivation half-lives ($t_{1/2}$) of reAuXyn10A, reATXyn10 and reATXyn10^{M} were measured, respectively, under the standard assay conditions except a temperature of 55 °C

when locust bean gum, guar gum or sodium carboxymethyl cellulose was used as the substrate. The K_m values of reATX10A and reATX10A^{M}, towards birchwood xylan at pH 5.5 and 50 °C for 15 min, were graphically determined to be 2.2 and 2.16 mg/ml, respectively, which were similar to that (2.25 mg/ml) of reAuXyn10A. Their V_{max} values were 5,924 and 8,870 U/mg, respectively. The reATX10A^{M} displayed a significant increase in V_{max} value as compared with the reAuXyn10A [26] which might be caused by the significant increase of its thermostability at 50 °C.

Analysis of the 3-D structures of AuXyn10A and ATX10A^{M}

The polar surface area (PSA) of a macromolecule was defined as the surface area sum over all polar atoms [7]. Previous research demonstrated that the PSA of a molecule

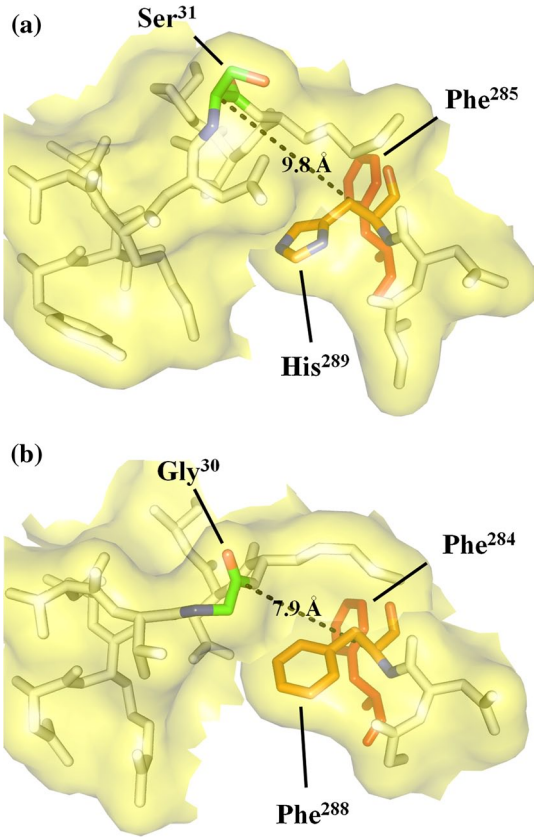

Fig. 8 Analysis and comparison between the local 3-D structures of AuXyn10A (**a**) and ATXyn10^{M} (**b**) using the PIC server. The C_{α}-atomic distance between Ser^{31} and His^{289} of AuXyn10A was compared with that between Gly^{30} and Phe^{288} of ATXyn10^{M}. An additional hydrophobic interaction between Phe^{284} and Phe^{288} was introduced into ATXyn10^{M} by mutating His^{289} into Phe^{288}

was positively correlated to its thermostability because of its potential interactions with solvent [13, 25]. In this work, the PSA of ATXyn10^{M} calculated using the GetArea program was 4,624.0 Å^2, larger than that (4,528.2 Å^2) of AuXyn10A. The increased PSA of ATXyn10^{M} may be caused by substituting the YP from Tyr^{25} to Pro^{34} of AuXyn10A with the corresponding one from Asn^{24} to Ala^{32} of TaXyn10 (Fig. 1).

The experimental results have revealed that both segment substitution and site-directed mutagenesis of AuXyn10A contributed to its elevated thermostability. To elucidate the thermostability mechanism, the intramolecular interactions relative to key amino acid residues of AuXyn10A and ATXyn10^{M} were identified and compared, respectively, using the PIC server (Fig. 8). The C_{α}-atomic distance between Gly^{30} and Phe^{288} of ATXyn10^{M} shorten to 7.9 Å as compared with that (9.8 Å) between Ser^{31} and His^{289} of AuXyn10A. In addition, an additional intramolecular interaction between Phe^{284} and Phe^{288} was introduced into ATXyn10^{M} by mutating His^{289} of AuXyn10A into Phe^{288} of ATXyn10^{M}, which may improve its thermostability through enhancing the hydrophobic interaction.

Conclusions

Based on the in silico design, this work significantly improved the thermostability of a mesophilic AuXyn10A by both segment substitution and site-directed mutagenesis. The ATXyn10^{M}-encoding gene, *ATxyn10*^{M}, was constructed as designed theoretically, and expressed in *P. pastoris*. The temperature optimum of reATXyn10^{M} was 10 °C higher than that of reAuXyn10A. The $t_{1/2}$ of reATXyn10^{M} at 55 °C was 10.4-fold longer than that of reAuXyn10A. Compared with reAuXyn10A, reATXyn10^{M} displayed a significant increase in V_{max} value. This methodology by computational prediction for the xylanase thermostability also can be used as a practical tool for other enzyme thermostabilization.

Acknowledgments This work was supported by the National Nature Science Foundation of China (No. 31101229), Key Laboratory of Carbohydrate Chemistry and Biotechnology, Ministry of Education, Jiangnan University (No. KLCCB-KF201208), Doctoral Research Funds of Jiangnan University (No. JUDCF11032) and Postgraduate Innovation Training Project of Jiangsu (No. CXZZ12_0758). The authors are grateful to Prof. Xianzhang Wu (School of Biotechnology, Jiangnan University) for providing technical assistance.

References

1. Ahmed S, Riaz S, Jamil A (2009) Molecular cloning of fungal xylanases: an overview. Appl Microbiol Biotechnol 84:19–35
2. Badieyan S, Bevan DR, Zhang CM (2012) Study and design of stability in GH5 cellulases. Biotechnol Bioeng 109:31–44
3. Biely P, Vršanská M, Tenkanen M, Kluepfel D (1997) Endo-β-1,4-xylanase families: differences in catalytic properties. J Biotechnol 57:151–166
4. Cai HY, Shi PJ, Bai YG, Huang HQ, Yuan TZ, Yang PL, Luo HY, Meng K, Yao B (2011) A novel thermoacidophilic family 10 xylanase from *Penicillium pinophilum* C1. Process Biochem 46:2341–2346
5. Collins T, Gerday C, Feller G (2005) Xylanases, xylanase families and extremophilic xylanases. FEMS Microbiol Rev 29:2–23
6. Dumon C, Varvak A, Wall MA, Flint JE, Lewis RJ, Lakey JH, Morland C, Luginbuhl P, Healey S, Todaro T, DeSantis G, Sun M, Parra-Gessert L, Tan X, Weiner DP, Gilbert HJ (2008) Engineering hyperthermostability into a GH11 xylanase is mediated by subtle changes to protein structure. J Biol Chem 283:22557–22564
7. Ertl P, Rohde B, Selzer P (2000) Fast calculation of molecular polar surface area as a sum of fragment based contributions and its application to the prediction of drug transport properties. J Med Chem 43:3714–3717
8. Eswar N, Eramian D, Webb B, Shen MY, Sali A (2008) Protein structure modeling with MODELLER. Methods Mol Biol 426:145–159
9. Gao SJ, Wang JQ, Wu MC, Zhang HM, Yin X, Li JF (2013) Engineering hyperthermostability into a mesophilic family 11

xylanase from *Aspergillus oryzae* by in silico design of N-terminus substitution. Biotechnol Bioeng 110:1028–1038
10. Hakulinen N, Turunen O, Janis J, Leisola M, Rouvinen J (2003) Three-dimensional structures of thermophilic β-1,4-xylanases from *Chaetomium thermophilum* and *Nonomuraea flexuosa*: comparison of twelve xylanases in relation to their thermal stability. Eur J Biochem 270:1399–1412
11. Jaenicke R, Böhm G (1998) The stability of proteins in extreme environments. Curr Opin Struct Biol 8:738–748
12. Kabsch W, Sander C (1983) Dictionary of protein secondary structure: pattern recognition of hydrogen-bonded and geometrical features. Biopolymers 22:2577–2637
13. Knapp S, Kardinahl S, Hellgren N, Tibbelin G, Schäfer G, Ladenstein R (1999) Refined crystal structure of a superoxide dismutase from hyperthermophilic archaeon *Sulfolobus acidocaldarius* at 2.2 Å resolution. J Mol Biol 285:689–702
14. Li JF, Tang CD, Shi HL, Wu MC (2011) Cloning and optimized expression of a neutral endoglucanase gene (*ncel5A*) from *Volvariella volvacea* WX32 in *Pichia pastoris*. J Biosci Bioeng 111:537–540
15. Lo Leggio L, Kalogiannis S, Bhat MK, Pickersgill RW (1999) High resolution structure and sequence of *T. aurantiacus* xylanase I: implications for the evolution of thermostability in family 10 xylanases and enzymes with (beta)alpha-barrel architecture. Proteins 36:295–306
16. Luo HY, Yang J, Li J, Shi PJ, Huang HQ, Bai YG, Fan YL, Yao B (2010) Molecular cloning and characterization of the novel acidic xylanase XYLD from *Bispora* sp. MEY-1 that is homologous to family 30 glycosyl hydrolases. Appl Microbiol Biotechnol 86:1829–1839
17. Miyazaki K, Takenouchi M (2002) Creating random mutagenesis libraries using megaprimer PCR of whole plasmid. Biotechniques 33:1033–1034
18. Pastor FIJ, Gallardo O, Sanz-Aparicio J, Diaz P (2007) Xylanases: molecular properties and applications. In: Polaina J, MacCabe AP (eds) Industrial enzymes. Springer, Germany, pp 65–82
19. Purmonen M, Valjakka J, Takkinen K, Laitinen T, Rouvinen J (2007) Molecular dynamics studies on the thermostability of family 11 xylanases. Protein Eng Des Sel 20:551–559
20. Radestock S, Gohlke H (2008) Exploiting the link between protein rigidity and thermostability for data-driven protein engineering. Eng Life Sci 8:507–522
21. Reetz MT, Carballeira JD (2007) Iterative saturation mutagenesis (ISM) for rapid directed evolution of functional enzymes. Nat Protoc 2:891–903
22. Reetz MT, Carballeira JD, Vogel A (2006) Iterative saturation mutagenesis on the basis of B factors as a strategy for increasing protein thermostability. Angew Chem Int Ed 45:7745–7751
23. Sunna A, Bergquist PL (2003) A gene encoding a novel extremely thermostable 1,4-β-xylanase isolated directly from an environmental DNA sample. Extremophiles 7:63–70
24. Vardakou M, Flint J, Christakopoulos P, Lewis RJ, Gilbert HJ, Murray JW (2005) A family 10 *Thermoascus aurantiacus* xylanase utilizes arabinose decorations of xylan as significant substrate specificity determinants. J Mol Biol 352:1060–1067
25. Vieille C, Zeikus GJ (2001) Hyperthermophilic enzymes: sources, uses, and molecular mechanisms for thermostability. Microbiol Mol Biol Rev 65:1–43
26. Wang JQ, Yin X, Wu MC, Zhang HM, Gao SJ, Wei JT, Tang CD, Li JF (2013) Expression of a family 10 xylanase gene from *Aspergillus usamii* E001 in *Pichia pastoris* and characterization of the recombinant enzyme. J Ind Microbiol Biotechnol 40:75–83
27. Wang JQ, Zhang HM, Wu MC, Tang CD (2011) Cloning and sequence analysis of a novel xylanase gene, *Auxyn10A*, from *Aspergillus usamii*. Biotechnol Lett 33:1029–1038
28. Yoon HS, Han NS, Kim CH (2004) Expression of *Thermotoga maritima* endo-β-1,4-xylanase gene in *E. coli* and characterization of the recombinant enzyme. Agric Chem Biotechnol 47:157–160
29. Zhang HM, Li JF, Wang JQ, Yang YJ, Wu MC (2014) Determinants for the improved thermostability of a mesophilic family 11 xylanase predicted by computational methods. Biotechnol Biofuels 7:3